

## Article

# Validated Analytical Modeling of Eccentricity and Dynamic Displacement in Diesel Engines with Flexible Crankshaft

Salah A. M. Elmoselhy <sup>1,\*</sup>, Waleed F. Faris <sup>2</sup> and Hesham A. Rakha <sup>3</sup><sup>1</sup> CFisUC, Department of Physics, University of Coimbra, P-3004 516 Coimbra, Portugal<sup>2</sup> Department of Mechanical Engineering, International Islamic University Malaysia, Gombak, Kuala Lumpur 53100, Malaysia<sup>3</sup> Virginia Tech Transportation Institute, Virginia Polytechnic Institute and State University, 3500 Transportation Research Plaza, Blacksburg, VA 24061, USA

\* Correspondence: salah.elmoselhy@msm.nl

**Highlights:**

- Analytically modeling the effect of eccentricity on flexible crankshaft and piston secondary motion;
- Analytically modeling the eccentricity of the crankshaft;
- Analytically modeling the absolute value of the dynamic displacement of the center of the crankshaft;
- Showing how sensitive the dynamic displacement in flexible crankshafts is to the changes in its independent variables;
- Double experimental validation of the analytical models based on the eccentricity of the crankshaft and based on fatigue analysis;
- A proposed approach of fatigue failure analysis for vehicular dynamic components;
- A proposed nanostructure of crankshafts for improved structural mechanics.



**Citation:** Elmoselhy, S.A.M.; Faris, W.F.; Rakha, H.A. Validated Analytical Modeling of Eccentricity and Dynamic Displacement in Diesel Engines with Flexible Crankshaft. *Energies* **2022**, *15*, 6083. <https://doi.org/10.3390/en15166083>

Academic Editor: Adrian Ilinca

Received: 1 February 2022

Accepted: 29 April 2022

Published: 22 August 2022

**Publisher's Note:** MDPI stays neutral with regard to jurisdictional claims in published maps and institutional affiliations.



**Copyright:** © 2022 by the authors. Licensee MDPI, Basel, Switzerland. This article is an open access article distributed under the terms and conditions of the Creative Commons Attribution (CC BY) license (<https://creativecommons.org/licenses/by/4.0/>).

**Abstract:** In spite of the fact that the flexibility of the crankshaft of diesel engines exhibits notable nonlinearities, analytical modeling of such nonlinearities is not yet realized. The present study thus analytically models the effect of eccentricity on flexible crankshaft and piston secondary motion. The eccentricity of the crankshaft is modeled as the summation of the hydrodynamic eccentricity and the dynamic mass eccentricity of the crankshaft. The study also models the absolute value of the vibrational dynamic displacement of the center of the crankshaft. The paper proves that such dynamic displacement of the center of the crankshaft is sensitive to the changes in its independent variables. It was found that the most influential parameters on the dynamic displacement of the center of the crankshaft due to vibration are the natural frequency and the eccentricity of the crankshaft. The modeling of the dynamic displacement in a flexible crankshaft was validated using a case study based on the eccentricity of the crankshaft showing a relative error of 4%, which is less than the relative error in the CMEM and GT-Power. Furthermore, the analytical modeling of the dynamic displacement in the flexible crankshaft was validated using another case study based on fatigue analysis of the crankshaft showing a relative error of 9%, which is less than that the relative error in Newman's model of diesel engine fuel consumption and Lansky's model of diesel engine cylinders. The paper also presents a proposed approach of fatigue failure analysis for vehicular dynamic components and presents a proposed nanostructure of crankshafts for improving such fatigue performance. The developed models would help develop efficient diesel engines and help prolong their service life.

**Keywords:** analytical modeling; flexible crankshaft; mechanics of materials; fatigue; tribology; diesel engine; sustainability

## 1. Introduction

The crankshaft is one of the most vintage inventions that are still in wide use. The analytical modeling of automotive components that are integrated with crankshafts is favor-

ably adopted in automotive and environmental engineering research [1]. The significance of analytical modeling becomes more apparent in light of the fact that the core and subroutines of the computational modelers are based on analytical/semi-analytical models. Diesel engines development is continually favored because of the distinguished operating features diesel engines exhibit [2]. Such development enables slashing the noticeable and negative impact of diesel engines on air quality. As a key tool to developing diesel engines, modeling assumes a key role in such development [3]. The powerful efficiency of the modeling tool has several key applications, such as Intelligent Transportation Systems (ITS) [4,5]. Some studies addressed what influences diesel engines' in-cylinder pressure, such as [6,7]. The present paper thus analytically investigates the modeling of the eccentricity and dynamic displacement in diesel engines taking the flexibility of the crankshaft into account.

The crankshaft converts the linear reciprocating motion of the piston into a rotary motion with a four-link mechanism, which is formed by the offset in the rod bearings and crank. The crankshaft is subjected to torsional loads due to the inertia of rotating components resulting in shear stresses, and is also subjected to bending loads due to gas pressure resulting in compressive and tensile stresses. Due to reversible cyclic loadings, these stresses become fatigue stresses. Fatigue is the primary cause of failure of crankshafts in internal combustion engines [8].

Eccentricity is also an important aspect to be taken into account in the modeling and analysis of internal combustion engines. Hongwei et al. analyzed crankshaft offset due to piston movement [9]. Particularly, they investigated through numerical modeling the relationship between the crankshaft offset value and piston noise. They also analyzed the effect of crankshaft bias on the impact energy of the piston. They found that larger positive crankshaft bias can simultaneously reduce piston secondary motions and piston noise. They also found that larger positive crankshaft bias reduces the impact energy and piston skirt friction loss. However, they did not analytically model the total energy and eccentricity in the crankshaft. Milasinovic et al. [10] further determined the journal's central position relative to the bearings of the crankshaft of a reciprocating engine. They used a Finite Element Analysis (FEA) for determining the trajectory of the journal's center. They showed that the trajectory of the journal's center is a function of the ratio of the eccentricity of the bearing's center to the installation clearance of the crankpin journal.

From the tribological perspective, the eccentricity of flexible crankshaft is considered in relation to its journal bearing. Journal bearings meritoriously exhibit high load carrying capacity and superior durability. The eccentricity of the flexible crankshaft is significantly affected by the eccentricity of the journal of the supporting bearing. The operational regime of the journal bearing affects the eccentricity of the flexible crankshaft.

Dynamic displacement is another pertinent factor in the modeling and analysis of diesel engines. Fonte et al. adopted an experimental approach, using vibrations analysis and Scanning Electron Microscopy (SEM) analysis to investigate the failure mode of a diesel engine's crankshaft [11]. They found that the cause of failure was a crack propagated at the crankpin web-fillet and emphasized that fatigue was the key failure mechanism. They also found that misalignment of the main journal of the crankshaft in its assembly was the root cause of the initiation of the crack. However, their research did not provide analytical modeling of the frequency-based aspects of the crankshaft. Kim and Lee [12] also investigated dynamic displacement in the crankshaft. They measured the concentrated stress at the crankpin fillet using a rosette gage located at  $45^\circ$  from an axis parallel to the crankshaft axis in the elevation view. They determined the fatigue strength of the crankshaft based on the measured strain in the gage. They found that the area of the highly dynamical stresses in the crankshaft is located near the crankpin. Giakoumis et al. studied crankshaft torsional deformation in turbocharged diesel engines under steady-state and transient operations [13]. They developed an analytical model of the torque in the crankpin of the crankshaft. They thus figured out the underlying mechanism of crankshaft torsional deformations during steady-state and transient operations by relating the torque to the rotational speed. Their study validated their analytical model using a case study. The

study concluded that deformation can become considerable, depending on the engine-load configuration (load variations and crankshaft stiffness). However, that analytical model did not provide analytical modeling of the eccentricity of the crankshaft. In fact, there is currently a tendency to increase cylinder pressure in order to increase mechanical efficiency, for instance, by utilizing the pressure of the intake compressor [14]. However, such an approach can negatively affect, tribologically, the building-up and development of lubricating oil film thickness in the flexible crankshaft and the piston/cylinder assembly [15].

Rakha et al. [16] pointed out recently that a widely valid model of diesel engines is sought for evaluating current/new diesel engines technologies. Faris et al. [17] therefore analytically modeled the intake manifold of supercharged diesel engines considering the crankshaft of the engine as an inflexible shaft. However, that modeling endeavor did not take into account the flexibility of the crankshaft, although the flexibility of the crankshaft in diesel engines can exhibit significant nonlinearities in the dynamics of diesel engines. More recently, Faris et al. [6] analytically modeled the intake manifold of supercharged diesel engines considering the crankshaft of the engine as a flexible shaft. Though analytical modeling of vehicular components describes the physical phenomena associated with vehicle's operation based on the principles of physics and with explainable mathematical trends, no analytical model has been developed, as yet, of the frequency-based aspects and eccentricity of the crankshaft taking into account the flexibility of crankshaft. Hence, the main idea of the present paper is to develop and validate an analytical model of the eccentricity and dynamic displacement in diesel engines taking the flexibility of the crankshaft of engines into account. The present research investigation also investigates the fatigue failure of such vehicular dynamic components as crankshafts and the improvement of the nanostructure of crankshafts for improved structural mechanics.

## 2. Brief Review on the Tribological Aspects and Mechanics of Materials of Diesel Engines

The tribological aspects and the mechanics of materials are related to each other. They affect the performance of the components of the diesel engine. The cyclic material properties are used to estimate the rate at which fatigue stresses accumulate during each cycle.

Currently, the major crankshaft material options are nodular cast iron and forged alloy steel (e.g., the standard SAE-4340), in which the carbon content is the main determinant of the ultimate strength and hardness to which such an alloy can be heat-treated [8]. High strength steels are refined for removing undesirable impurities such as sulfur and phosphorus [18].

There is another ultra-high strength and impact resilient class of steel, "maraging steel", which is not based on carbon, but rather is based on nickel and on crystalline phase transformation due to age-hardening and the precipitation of intermetallic compounds [19]. However, maraging steel is not frequently used in fabricating crankshafts because of the high cost of removing the significant distortions which occur during the nitriding soak in case hardening. Very shallow case hardening does not allow for a smooth gradient of hardness from the surface to the core of the shaft, which results in drastically degrading the fatigue and impact properties of the steel.

Williams and Fatemi [20] performed fatigue behavior evaluation on the forged steel (AISI 1045) and ductile cast iron crankshaft material. They observed that under cyclic loading: (i) the forged steel is cyclically softened, and (ii) the ductile cast iron is cyclically hardened. Patil et al. found that most crankshaft failures are due to fatigue loading and stress concentration resulting in crack formation and, consequently, failure [21]. Bhosale et al. investigated crankshafts made of nodular cast iron, austempered ductile iron, forged steel, and micro-alloyed forged steel [22]. They concluded that fatigue is the dominant mechanism of failure of the crankshaft. Industrially, DNV GL Corporation provided guidelines that contain analytical methods for designing for fatigue resilient crankshafts in the industry [23]. These methods include: stresses calculations, evaluation of stress concentration factors, and the acceptability criteria.

Aliakbaria et al. experimentally and numerically investigated how significant fatigue function and failure in the crankshaft of the diesel engine of heavy trucks are [24]. They concluded that the fatigue failure resulting from the bending-torsional load-combination is chiefly due to material-related aspects. Witek et al. found that the chief mechanism of crankshaft failure is the fatigue of material [25]. The high-cycle fatigue conditions deteriorated the crankpin fillets, resulting in an unbalanced shaft which in turn excited the resonant frequency of the crankshaft and thus shortened the fatigue life of the crankshaft. They recommended the fillet rolling process on crankpin fillets for inducing compressive stresses that can increase the number of load cycles to crack initiation.

Industrially, KOBELCO found that the most important characteristic of a crankshaft is the fatigue strength of the crankpin fillets [26]. Kubo and Mori [26] also recommended improving fatigue strength by cold rolling the fillets. They found that a significant improvement in fatigue strength is obtained by cold rolling, which causes work-hardening and compressive residual stresses onto the material surface. There are thus mainly four methods of fabricating crankshafts: (i) hot rolling/forging, (ii) mold-based casting, (iii) machining (Turning/Milling), and (iv) rapid prototyping that includes rapid fabrication directly from CAD data by additive manufacturing with layers deposition for reducing cost and time [27].

From the tribological stand-point, journal bearings operate in three regimes: the boundary regime, the mixed regime, and the hydrodynamic regime. Journal bearings operate in the boundary regime (metal-to-metal contact) only during the startup and shutdown of the equipment when the rotational speed of the journal is insufficient to generate and build an oil film. It is during the startup and shutdown when most of the damage to the journal bearings occurs [28,29]. The mixed lubrication regime describes the transition between the pure hydrodynamic lubrication regime, where a fluid separates the contacting surfaces, and the boundary lubrication regime, where the metal-metal contact is significant. In the mixed lubrication regime, the fluid film cannot completely separate the adjacent surfaces, so that the hydrodynamic and asperity friction phenomena coexist. The friction coefficient finds its minimum at the transition between the mixed lubrication and the hydrodynamic lubrication [30]. The designers of journal bearings often aim for minimizing the amount of exposure of the journal bearing to the severe lubrication mode, “mixed friction”, where significant wear occurs, since most drops in friction torque occur in this operational regime [30]. The hydrodynamic fluid film allows these journal bearings to support extremely heavy loads and operate at high rotational speeds [28,29].

The lubrication mode is affected by the viscosity of the lubricant, wettability, and oil film thickness. Oils are used in journal bearings when cooling is required, friction needs to be minimized, and/or debris needs to be flushed away from the bearing. High-speed journal bearings are always lubricated with oil rather than grease. The higher the bearing speed, the lower the required viscosity of the oil will be; the higher the operating temperature of the unit will be, the higher the required viscosity of the oil will be. If the selected oil is too low in viscosity, heat will develop due to an insufficient film thickness and some metal-to-metal contact will occur. If the oil is too high in viscosity, heat will again be generated, but due to the internal fluid friction generated within the oil. Selecting the oil that is too high in viscosity can also increase the likelihood of cavitation. Cavitation is a result of the expansion of dissolved air or water vapor in the low-pressure zone of the bearing. The resulting bubble implodes, causing damage whilst passing through the high-pressure portion of the bearing [28,29].

Key rheological properties of lubricants, such as viscosity, depend on operating temperature, pressure, and shear rate [30]. Although thermal effects affect elastic deformation, which in turn influences the hydrodynamic lubrication of the bearing, the temperature rise within the journal is basically about 60 °C [30].

Advancements in materials science have been utilized for improving the performance of journal bearings. Notably, 2D materials, such as graphene and *h*-BN, have shown outstandingly low frictional coefficients and wear rates, so that they have become attractive materials for high-performance nano-lubricants and lubrication applications [31]. Several

common 2D materials have tribological applications, such as their use as solid lubricants and lubricant nano-additives. Modifying an oil lubricant with an additive solid lubricant, such as Molybdenum Disulfide ( $\text{MoS}_2$ ), by a very small percentage (smaller than 1 wt.%) can result in reducing the coefficient of friction and the size of the wear scar by up to 37% and 16%, respectively [31]. In addition, boron nitride (BN) has been found to consist of a similar structural lattice to the carbons of graphene; as such, *h*-BN powder is often used as a solid lubricant [32].

The presence of a coating on friction surfaces and the addition of nanoparticles into mineral oil lubricants have an integrative effect towards significantly reducing the friction coefficient and the wear rate [33]. However, some challenges limit their wide industrial application. A key challenge that faces the 2D materials is the lack of dispersion in lubricating oil. Nanomaterials like graphene nanosheets and  $\text{WS}_2$  often agglomerate in lubricants due to high surface ratios and significant van der Waals forces [31].

Several innovations have been proposed for improving the performance of journal bearings. Some researchers proposed dividing the journal bearing surface into the heterogeneous surface condition of a slip boundary condition zone and a nonslip boundary condition zone. This can maximize tribological benefits for critical shear stress in order to minimize wear rate [34]. Other researchers suggested to use a tilting-pad bearing for self-adjusting operations of the journal bearing, and thus reducing wear. The tilting-pad bearing has the ability to tilt in order to accommodate the forces that develop in the hydrodynamic oil film and, therefore, operates with an optimum oil-film thickness for the given load and speed [35]. Others suggested to have surface textures of rectangular grooves on the contact surface of the journal bearing for improving the heat dissipation during operations [36]. This is in accord with the phenomenon of laminar-turbulent flow transition in high-load regions of the fluid film, which directly reduces the maximum oil-film temperatures and thus enables extending the operating load limits of the journal bearing [35]. Several researchers suggested to use dry-running journal bearings, such as metal-polymer composite bearing bushings, e.g., polyamides [37]. The temperature affects the elastic characteristics of polymeric materials such that, as the temperature increases during operations, the polymers become more deformable. A decrease in the value of the Young's modulus of the polymeric composites results in a decrease in the level of the initial maximum contact pressures. This increases the bearing capacity of the bearing by up to 10% [37]. Amongst these dry-running journal bearings are porous metal plain bearings that are oil-impregnated. The potential use of these bearings is limited to low-load and low-surface speed applications. Semi-lubricated journal bearings often consist of a shaft rotating in a porous metal sleeve of sintered bronze or aluminum in which lubricating oil is contained within the pores of the sleeve [28,38]. Such dry-running journal bearings, meritoriously, are basically maintenance-free [29].

### 3. Research Methodology

The present research work is quantitative research based on a theoretical approach employing exploratory and descriptive techniques for analytical modeling: (a) how eccentricity in the flexible crankshaft affects crankshaft and piston secondary motion, (b) the eccentricity of the crankshaft as the summation of the hydrodynamic eccentricity and dynamic mass eccentricity of the crankshaft, and (c) the absolute value of the vibrational dynamic displacement of the center of the flexible crankshaft. The experimental data for validation have been collected from the literature in two case studies for validating the developed analytical models. The proposed approach of fatigue failure analysis for vehicular dynamic components is based on analytical modeling derived from the principles of physics. Computational finite element models have been built in this research for validating the proposed nanostructure of the crankshaft for improved structural mechanics. The strength and the corresponding induced stresses of the proposed nanostructure of the crankshaft have been computationally modeled using finite element analysis based on the COMSOL Multiphysics modeler.

The following contributions are accomplished in this paper:

- (i) Analyzing the effect of eccentricity in the flexible crankshaft on crankshaft and piston secondary motion (Section 4);
- (ii) Analytically modeling the eccentricity of the crankshaft as the summation of the hydrodynamic eccentricity and the dynamic mass eccentricity of the crankshaft (Section 4);
- (iii) Analytically modeling the absolute value of the vibrational dynamic displacement of the center of the crankshaft (Section 5);
- (iv) A sensitivity analysis based on the developed analytical model of the dynamic displacement in flexible crankshafts has been conducted (Section 6);
- (v) Analytical modeling of the dynamic displacement in the flexible crankshaft has been validated using an experimental case study based on the eccentricity of the crankshaft showing a relative error of 4% (Section 7);
- (vi) Analytical modeling of the dynamic displacement in the flexible crankshaft has been validated using another experimental case study based on fatigue analysis showing a relative error of 9% (Section 8);
- (vii) A proposed approach of fatigue failure analysis for vehicular dynamic components (Section 9);
- (viii) A proposed nanostructure of the crankshaft for improved structural mechanics (Section 10).

#### 4. Effect of Eccentricity in the Flexible Crankshaft on Crankshaft and Piston Secondary Motion

The crankshaft has its own torsional stiffness that causes it to have its own torsional resonant frequency. The cyclic torque's peaks and valleys along with the inertial loads from the acceleration of the reciprocating components constitute vibrational excitations that cause the crankshaft to rotationally deflect during operation. When those excitations are near the crankshaft's resonant frequency, they can cause the crankshaft to eventually break. A key objective in designing crankshafts is to chiefly separate the crankshaft torsional resonance point away from the excitation frequencies of operation of the crankshaft. Crankshaft length and main journal diameter are major factors in deciding the torsional stiffness of a crankshaft.

First order or first harmonic balance is supposed to indicate the balancing of items that could shake an engine once in every rotation of the crankshaft, i.e., having the frequency equal to one crank shaft rotation. For example, a single cylinder engine with no balance shafts. Second order balance is twice the frequency in one crank rotation. For a conventional inline four-cylinder engine, the two outer pistons are 180° opposed to the inners so that the outers are at the bottom dead center (BDC) and the inners are at the top dead center (TDC). When the pistons are at BDC/TDC, the connecting rods are straight up and down. When the crankshaft position is mid-travel, the pistons are not at the mid-position, and the connecting rods are hence at an angle to the side. This happens twice per revolution, so the resulting vertical vibration is at double the crank rotation frequency. Thus, there is one speed of rotation of the crankshaft and more than one frequency of vibration response for the various components associated with the crankshaft.

The mass flow rate of the air that goes from intake manifold into all the cylinders of the engine,  $\dot{m}_{AC}$ , is a function of crankshaft rotational speed. Crankshaft rotational speed is a function of the instantaneous and linear velocity of the piston, which is in turn a function of the geometry of the crank and connecting rod assembly. Hence, the  $\dot{m}_{AC}$  may be affected if the crankshaft is flexible. The key condition of flexibility is as follows:

$$\omega_c \geq \omega_n \quad (1)$$

where:  $\omega_c$  is the operating speed of rotation of the crankshaft (rad/s).  $\omega_n$  is the natural frequency of the crankshaft (rad/s).

Equation (1) can be rewritten as follows, based on the definition of the natural frequency:

$$\omega_c \geq \sqrt{K_c/m_c} \quad (2)$$

where:  $K_c$  is the stiffness of the crankshaft (N/m).  $m_c$  is the mass of the crankshaft and its associated components (kg).

Crankshafts most often run based on fluid film bearings. These journal bearings operate by generating a thin film of a lubricant at a relatively high pressure to match the load due to the relative motion between the shaft and the bearing, as shown in Figure 1. These bearings operate in three modes: (a) fully-hydrodynamic, (b) boundary, and (c) mixed [39,40]. From a tribological perspective, the difference between the maximal and minimal wall thickness of the hydrodynamic wedge of the main journal bearing of the crankshaft is directly related to the hydrodynamic eccentricity ( $e_{HD}$ ). In accord with the theory of lubrication proposed by Osborne Reynolds, the journal cannot keep a central position in the bearing but rather takes up a position based on its speed and load so that the conditions for equilibrium are satisfied. At high speeds, the eccentricity of the journal decreases, while at low speeds, this eccentricity increases. During the loading operation of the journal bearing, the pressurized lubricant therefore has to force its way through the narrow gap between the bearing and the journal, so that friction increases [41]. As the rotational speed gets higher, the lubricating film develops and increases, the lubricating fluid flow gets turbulent, the lubricating wedge develops, and the lubrication regime becomes hydrodynamic. Hydrodynamic eccentricity ( $e_{HD}$ ) can be formulated as [41,42]:

$$e_{HD} = \frac{(t_{WMax} - t_{WMin})}{2} \quad (3)$$

where:  $t_{WMax}$  is the maximal wall thickness of the hydrodynamic wedge of the main journal bearing of the crankshaft (m).  $t_{WMin}$  is the minimal wall thickness of the hydrodynamic wedge of the main journal bearing of the crankshaft (m).

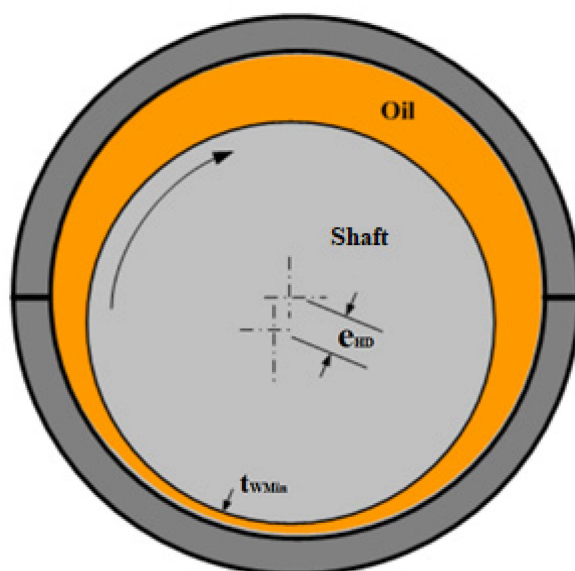


**Figure 1.** Hydrodynamic eccentricity in the journal bearing of the crankshaft.

The minimal wall thickness of the hydrodynamic wedge of the main journal bearing of the crankshaft ( $t_{WMin}$ ) can be analytically formulated as [42]:

$$t_{WMin} = C_{rc} - e_{HD} \quad (4)$$

where:  $C_{rc}$  is the radial clearance between the main journal and its bearing when the journal is placed centrally (m). The  $C_{rc}$  is a key characteristic of the journal bearing that is standardly provided for each journal bearing.

Likewise, the maximal wall thickness of the hydrodynamic wedge of the main journal bearing of the crankshaft ( $t_{WMax}$ ) can be analytically formulated as [42]:

$$t_{WMax} = C_{rc} + e_{HD} \quad (5)$$

The minimal wall thickness of the hydrodynamic wedge of the main journal bearing of the crankshaft ( $t_{WMin}$ ) can be also formulated as [41]:

$$t_{WMin} = \frac{4.9 \mu_o \omega_J r_J^2}{w_N} \quad (6)$$

where: 4.9 is a constant referring to a rigid, solid journal with iso-viscous lubricant.  $\mu_o$  is the lubricant viscosity at inlet conditions.  $\omega_J$  is the rotational speed of the journal.  $r_J$  is the relative radius of curvature of the contacting surfaces, which is basically the radius of the journal.  $w_N$  is the normal load carried by the bearing per unit width of the contact that carries the load.

It is noteworthy that the width of contact that carries the load imposed onto the journal bearing is basically  $\pi R_B$ , where  $R_B$  is the radius of the bearing, which equals  $(r_J + C_{rc})$  [43]. The effect of the tangential drag or shear stress upon the load is very small when compared with that of the normal pressure intensity and therefore may be neglected. This is a well-established assumption, since the error involved is of the order  $(C_{rc}/R_B)$ , i.e., less than 10% [41].

Hydrodynamic eccentricity ( $e_{HD}$ ) can thus be analytically modeled, following from the combination of Equations (4) and (6):

$$e_{HD} = C_{rc} - \frac{4.9 \mu_o \omega_J r_J^2}{w_N} \quad (7)$$

This hydrodynamic eccentricity of the crankshaft ( $e_{HD}$ ) produced by the varying wall thickness of hydrodynamic lubrication adds to the dynamic mass eccentricity of the crankshaft ( $e_{DM}$ ) for developing the eccentricity of the crankshaft ( $e_c$ ):

$$e_c = e_{HD} + e_{DM} \quad (8)$$

The dynamic mass eccentricity of the crankshaft ( $e_{DM}$ ) can be analytically determined using the algebraic formulation of the center of mass of the masses collectively associated with the crank of the crankshaft under consideration ( $m_R$ ). Let us call the Cartesian coordinate of the geometric center of symmetry of the crankshaft ( $x_o, y_o$ ). These masses are: (i) mass of the counterweight ( $m_{CW}$ ), which has its center of mass located at  $(e_{xCW}, e_{yCW})$  with respect to  $(x_o, y_o)$ , (ii) mass of connecting rod ( $m_{CR}$ ), which has its center of mass located at  $(e_{xCR}, e_{yCR})$  with respect to  $(x_o, y_o)$ , and (iii) mass of piston ( $m_P$ ), which has its center of mass located at  $(e_{xP}, e_{yP})$  with respect to  $(x_o, y_o)$ . Thus, the  $e_{DM}$  can be analytically formulated as:

$$e_{DM} = \sqrt{\left(\frac{m_P e_{xP} + m_{CR} e_{xCR} + m_{CW} e_{xCW}}{m_P + m_{CR} + m_{CW}} - x_o\right)^2 + \left(\frac{m_P e_{yP} + m_{CR} e_{yCR} + m_{CW} e_{yCW}}{m_P + m_{CR} + m_{CW}} - y_o\right)^2} \quad (9)$$

For  $(x_o, y_o)$  being the origin of the Cartesian coordinates, the relative  $e_c$  with respect to  $(x_o, y_o)$  is formulated by substituting Equations (7) and (9) in Equation (8):

$$e_c = \frac{\left[ C_{rc} - \frac{4.9 \mu_o \omega_J r j^2}{w_N} \right]}{\sqrt{\left( \frac{m_P e_{xP} + m_{CR} e_{xCR} + m_{CW} e_{xCW}}{m_P + m_{CR} + m_{CW}} \right)^2 + \left( \frac{m_P e_{yP} + m_{CR} e_{yCR} + m_{CW} e_{yCW}}{m_P + m_{CR} + m_{CW}} \right)^2}} \quad (10)$$

Analytically modeling the eccentricity of the crankshaft ( $e_c$ ) paves the way for analytically modeling the dynamic displacement of the center of the crankshaft,  $|D_c|$ .

### 5. Analytical Modeling of the Dynamic Displacement of the Center of Crankshaft $|D_c|$

From the perspective of vibrations, since the synchronous unbalance is the dominant type of imbalance in the crankshaft in the steady state, the phase angle of the whirling of the imbalance ( $\varphi$ ) is considered constant with respect to time. The dynamic displacement of the center of the flexible crankshaft due to vibration ( $x, y$ ) can be modeled based on the single degree of freedom forced vibration with damping, as shown in Figure 2. In this model, the operating speed of rotation of the crankshaft ( $\omega_c$ ) is the rate of change of the angle of rotation of the crankshaft ( $\alpha$ ).

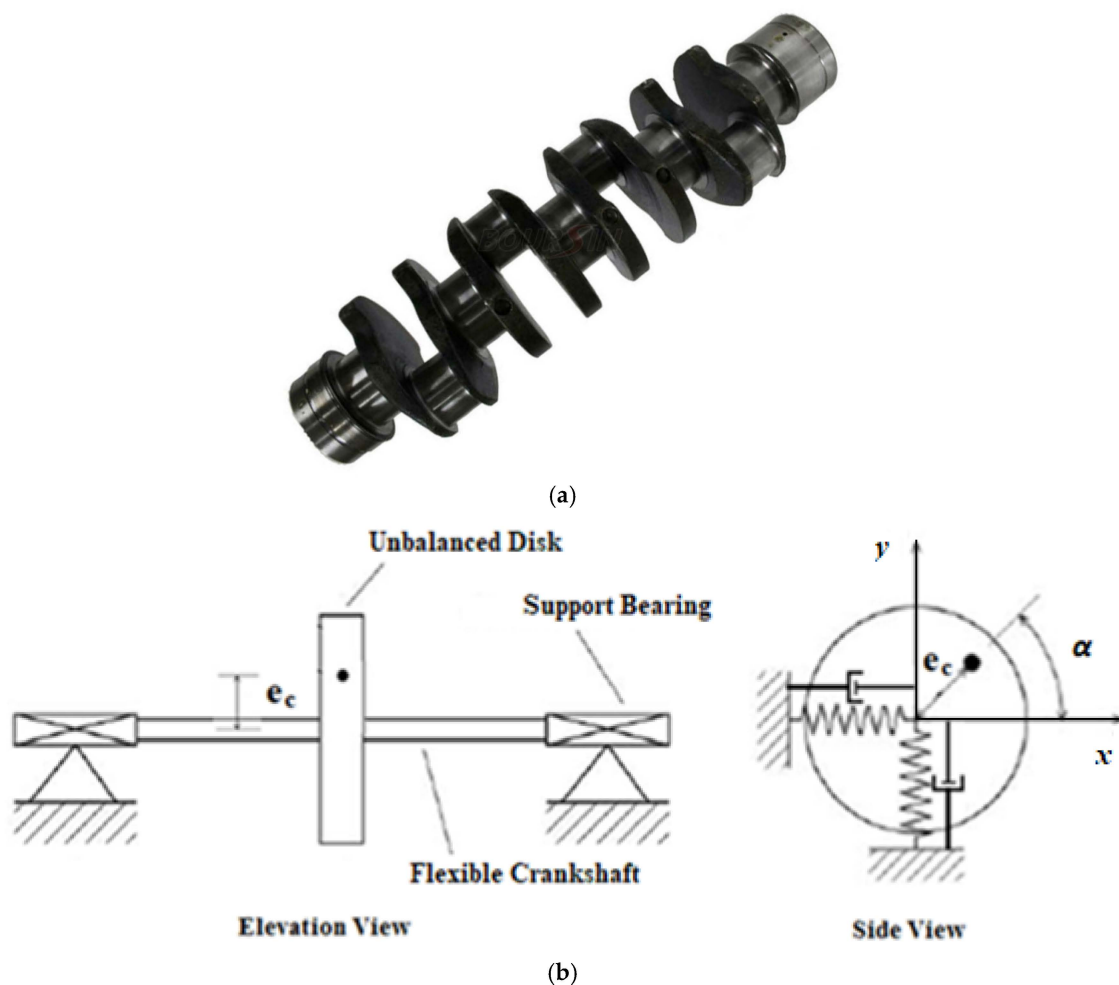


**Figure 2.** (a) A diesel four-cylinder engine crankshaft, Isuzu NPR NPS Truck 4HG1 Diesel Engine; (b) Schematic diagram of a flexible crankshaft of single-cylinder engine with unbalance.

Therefore, since the total force imposed onto the crankshaft has two components, a tangential component and radial component, the tangential and radial components of the centrifugal force generated due to unbalance in the crankshaft can be analytically modeled as:

$$F_{CT} = m_R \omega_c^2 e_c \cos \omega_c t \quad (11)$$

where:  $F_{CT}$  is the tangential component of the centrifugal force generated due to unbalance in the crankshaft (N).

$$F_{CR} = m_R \omega_c^2 e_c \sin \omega_c t \quad (12)$$

where:  $F_{CR}$  is the radial component of the centrifugal force generated due to unbalance in the crankshaft (N).

Thus, using the superposition principle in order to obtain the aggregate effect of the centrifugal force on flexible crankshaft dynamics, the equation of the vibrational motion for each direction is similar to those of the mass on a spring under the action of a periodic force with damping:

$$m_c \ddot{x} + c_c \dot{x} + K_c x = m_R \omega_c^2 e_c \cos \omega_c t \quad (13)$$

$$m_c \ddot{y} + c_c \dot{y} + K_c y = m_R \omega_c^2 e_c \sin \omega_c t \quad (14)$$

where:  $C_c$  is the damping coefficient in the crankshaft (kg·m/s).  $K_c$  is the flexible spring constant in the crankshaft (N/m).

Equations (13) and (14) can be transformed into one equation in one variable by using a complex variable ( $z$ ):

$$z = x + iy \quad (15)$$

where: the Euler's formula for the complex variable ( $z$ ) is [44]:

$$e^{i\omega_c t} = \cos \omega_c t + i \sin \omega_c t \quad (16)$$

Therefore, substituting Equations (15) and (16) into Equations (13) and (14):

$$m_c \ddot{z} + c_c \dot{z} + K_c z = m_R \omega_c^2 e_c e^{i \omega_c t} \quad (17)$$

Following from the definition of the damping ratio of the crankshaft ( $\zeta_c$ ):

$$\zeta_c = \frac{C_c}{2 \omega_n m_c} \quad (18)$$

Substituting Equations (2) and (18) into Equation (17), Equation (17) can hence be rewritten as:

$$\ddot{z} + 2 \zeta_c \omega_n \dot{z} + \omega_c^2 z = \frac{m_R}{m_c} \omega_c^2 e_c e^{i \omega_c t} \quad (19)$$

Since the synchronous unbalance is the dominant type of imbalance in the crankshaft in the steady state, the steady-state vibrational response is the dominant response. Hence, the influence of the term  $\omega_c^2 z$  in the steady-state vibrational response to forced vibration becomes insignificant. Since the external force is harmonic, the steady-state vibrational response by the harmonic forcing function is also harmonic. Thus, the solution to the equation of vibrational motion of the crankshaft (19) in the steady-state is:

$$z = D_c e^{i \omega_c t} \quad (20)$$

where:  $D_c$  is the complex amplitude of vibrational response of the crankshaft to be determined from the boundary conditions.

Hence the amplitude  $D_c$  can be formulated as:

$$D_c = \frac{e_c \omega_c^2}{(\omega_n^2 - \omega_c^2) + 2i \omega_c \omega_n \zeta_c} \quad (21)$$

By multiplying both the numerator and the denominator of the right-hand side of Equation (21) by the conjugate of the complex number of the denominator:

$$D_c = \frac{e_c \omega_c^2 [(\omega_n^2 - \omega_c^2) - 2i \omega_c \omega_n \zeta_c]}{(\omega_n^2 - \omega_c^2)^2 + (2 \omega_c \omega_n \zeta_c)^2} \quad (22)$$

Now, the complex amplitude of vibration response of the crankshaft ( $D_c$ ) has two components:

$$D_c = D_{cx} + i D_{cy} \quad (23)$$

where:  $D_{cx}$  is the x-component of the complex amplitude of vibration response of the crankshaft ( $D_c$ ),  $D_{cy}$  is the y-component of the complex amplitude of vibration response of the crankshaft ( $D_c$ ).

Thus, Equation (23) can be rewritten as:

$$D_c = |D_c| e^{i\phi} = \sqrt{D_{cx}^2 + D_{cy}^2} e^{i\phi} \quad (24)$$

Therefore, the absolute value of the dynamic displacement of the center of the crankshaft due to vibration  $|D_c|$  for SI units is:

$$|D_c| = \frac{e_c \omega_c^2}{\sqrt{(\omega_n^2 - \omega_c^2)^2 + (2 \omega_c \omega_n \zeta_c)^2}} \quad (25)$$

Thus, the phase angle of the dynamic displacement of the center of the crankshaft due to vibration  $\phi$  is:

$$\phi = \arctan \frac{2 \omega_c \omega_n \zeta_c}{\omega_n^2 - \omega_c^2} \quad (26)$$

Having modeled the dynamic displacement of the center of the crankshaft,  $|D_c|$ , analyzing how sensitive this developed model is to the changes in its independent variables follows.

## 6. Sensitivity Analysis of the Dynamic Displacement of the Center of the Crankshaft, $|D_c|$

In order to efficiently utilize the analytical model of the dynamic displacement of the center of crankshaft due to vibration  $|D_c|$ , its formula should be analyzed for testing how sensitive it is to the changes in its independent variables. This sensitivity analysis often further enables the simplification of the analytical model. This simplification is based on the sensitivity analysis of the models developed in the present study. The essence of this sensitivity analysis is to apply the sensitivity ratio,  $R_{Sensitivity}$ , which is formulated in Equation (27), to each of the independent variables. The  $R_{Sensitivity}$  is evaluated for each independent variable whilst maintaining the values of the remaining independent variables unchanged from the baseline values. The  $R_{Sensitivity}$  is formulated as follows [45]:

$$R_{Sensitivity} = \frac{\frac{v_{Dependent\ Changes} - v_{Dependent\ Baseline}}{v_{Dependent\ Baseline}}}{\frac{v_{Independent\ Changes} - v_{Independent\ Baseline}}{v_{Independent\ Baseline}}} \quad (27)$$

where:  $v_{Dependent\ Changes}$  is the value of the dependent variable in the analytical model with the increment/decrement of change.  $v_{Dependent\ Baseline}$  is the baseline value of the dependent variable in the analytical model.  $v_{Independent\ Changes}$  is the value of the independent variable in the analytical model with the increment/decrement of change.  $v_{Independent\ Baseline}$  is the baseline value of the independent variable in the analytical model. The dynamic displacement of the center of the crankshaft due to vibration,  $|D_c|$ , is analytically modeled in Equation (25). The key explanatory variable in this model is the damping ratio (i.e.,  $\zeta_c$ ). The baseline value of the ratio of ( $\zeta_c$ ) is "1". The sensitivity analysis of the analytical model of  $|D_c|$  is presented in Table 1 following from Equations (25) and (27).

**Table 1.** Sensitivity analysis of the analytical model of dynamic displacement,  $|D_c|$ .

	−50% Decrement Below Baseline Value	−25% Decrement Below Baseline Value	Baseline Value	+25% Increment Above Baseline Value	+50% Increment Above Baseline Value	Average Sensitivity Ratio on Each Independent Variable
$ D_c $	$0.005 * 10^{-3}$ m	$0.0075 * 10^{-3}$ m	$0.01 * 10^{-3}$ m	$0.0125 * 10^{-3}$ m	$0.0150 * 10^{-3}$ m	N/A
$e_c$	$0.04 * 10^{-3}$ m	$0.06 * 10^{-3}$ m	$0.08 * 10^{-3}$ m [46]	$0.10 * 10^{-3}$ m	$0.12 * 10^{-3}$ m	N/A
$R_{Sensitivity}$ , on $e_c$	1	1	N/A	1	1	1
$ D_c $	$0.005 * 10^{-3}$ m	$0.0075 * 10^{-3}$ m	$0.01 * 10^{-3}$ m	$0.0125 * 10^{-3}$ m	$0.0150 * 10^{-3}$ m	N/A
$\omega_c$	700 rpm	1050 rpm	1400 rpm [20]	1750 rpm	2100 rpm	N/A
$R_{Sensitivity}$ , on $\omega_c$	1	1	N/A	1	1	1
$ D_c $	$0.005 * 10^{-3}$ m	$0.0075 * 10^{-3}$ m	$0.01 * 10^{-3}$ m	$0.0125 * 10^{-3}$ m	$0.0150 * 10^{-3}$ m	N/A
$\omega_n$	1620 rpm	2430 rpm	3240 rpm [46]	4050 rpm	4860 rpm	N/A
$R_{Sensitivity}$ , on $\omega_n$	1	1	N/A	1	1	1

Thus, the  $|D_c|$  is sensitive to the changes in the value of  $e_c$ ,  $\omega_c$ , and  $\omega_n$ . Hence,  $e_c$ ,  $\omega_c$ , and  $\omega_n$  should not be considered a constant in the formulation of the  $|D_c|$ . The experimental validation of the developed model based on the eccentricity of the crankshaft ( $e_c$ ) is presented in the next section.

### 7. Experimental Validation of the Analytical Modeling of the Dynamic Displacement in Flexible Crankshaft $|D_c|$ Based on the Eccentricity of the Crankshaft ( $e_c$ )

The experimental validation of the analytical model of  $|D_c|$  developed in Equation (25) is presented in this section. A case study was conducted based on a 1-cylinder engine with a swept volume of 460 cc [20]. The field data that represent an operating point of rotational speed of 1400 rpm, which represents a near average speed of operating diesel engines and is near the rotational speed at maximum torque, are shown in Table 2 [47]. In this analysis, critical damping (i.e.,  $\zeta_c = 1$ ) is considered in this case, since that is the preferred dynamic response in the design of such a dynamic system.

**Table 2.** Field data on a case study conducted with respect to  $|D_c|$ .

Parameter	Value Extracted from Field Data	Reference
$ D_c $	$0.0096 * 10^{-3}$ m	[46,47]
$e_c$	$0.08 * 10^{-3}$ m	[46]
$\omega_c$	1400 rpm	[20]
$\omega_n$	3240 rpm	[46]

Based on Equation (25) and Table 2, the absolute value of the dynamic displacement of the center of the crankshaft due to vibration,  $|D_c|$ , is:

$$|D_c| = \frac{(0.08 * 10^{-3} \text{ m}) \left(1400 * \frac{2\pi \text{ rad}}{60 \text{ s}}\right)^2}{\sqrt{\left((339 \text{ rad/s})^2 - \left(1400 * \frac{2\pi \text{ rad}}{60 \text{ s}}\right)^2\right)^2 + \left(2 \left(1400 * \frac{2\pi \text{ rad}}{60 \text{ s}}\right) (339 \text{ rad/s}) (1)\right)^2}} = 0.01 * 10^{-3} \text{ m} \quad (28)$$

The statistical measure in this study is the relative error of the model,  $\varepsilon_R$ , which can be evaluated as follows [48]:

$$\varepsilon_R = \sum_{i=1}^{z_n} \left| \frac{y_i - x_i}{y_i} \right| \frac{100\%}{z_n} \quad (29)$$

where:  $y_i$  is the interval variable that is the measured value, i.e., field dataset.  $x_i$  is the interval variable that is the expected value analytically. The  $\varepsilon_R$  is utilized in this study as a

quantifiable measure of validation. The comparison of the data in this case study, which is based on the eccentricity of the crankshaft, ( $e_c$ ), with the results of the developed model of  $|D_c|$ , is statistically analyzed in Table 3 following from Equations (28) and (29).

**Table 3.** Summary of the statistical analysis of  $|D_c|$  based on the eccentricity of the crankshaft ( $e_c$ ).

Table #	$\bar{x}$	$\bar{y}$	$\epsilon_R$
Table 2	0.01 mm	0.0096 mm	4%

Further experimental validation of the developed model based on fatigue analysis follows.

### 8. Experimental Validation of the Analytical Modeling of the Dynamic Displacement in the Flexible Crankshaft $|D_c|$ Based on Fatigue Analysis

Since the crankshaft is a highly dynamic vehicular component, it is subjected to significant cyclic loadings. Thus, the fatigue analysis of the crankshaft is another significant aspect to be considered in the analysis and validation of the dynamic displacement in the flexible crankshaft. Thus, the developed analytical model of the dynamic displacement in the flexible crankshaft,  $|D_c|$ , is further validated in this section based on fatigue analysis using experimental data gathered from the literature. The cyclic stress strain curve can be described by the Ramberg–Osgood formula [49]:

$$\epsilon = \frac{\sigma}{E} + \left(\frac{\sigma}{K'}\right)^{\frac{1}{n'}} \quad (30)$$

where:  $\epsilon$  is the true strain,  $\sigma$  is the true stress,  $E$  is the modulus of elasticity,  $K'$  is the strength coefficient, and  $n'$  is the strain hardening exponent.

The true strain,  $\epsilon$ , is analytically formulated as [50]:

$$\epsilon = \ln\left(\frac{L_f}{L_o}\right) \quad (31)$$

where  $L_f$  is the final length of the crankshaft after the dynamic deformation, and  $L_o$  is the original length of the crankshaft.

Hence, based on the original geometry of the crankshaft, the original length of the crankshaft ( $L_o$ ) is considered to be the distance from the first crank to the first bearing, i.e., about 113 mm [46]. In addition, based on the analytical result obtained from the developed analytical model of the dynamic displacement of the center of the crankshaft due to vibration  $|D_c|$ , indicated in Equation (28), the final length of the crankshaft after dynamic deformation ( $L_f$ ) becomes about 0.113095 m, near the crank angle of maximum pressure in the cylinder,  $\alpha = 370^\circ$  where the vibrational effect, piston pressure and accelerated weight become significantly large. Therefore, substituting these values into Equation (31) leads to a true strain,  $\epsilon$ , of  $9 \times 10^{-4}$ . Thus, the true stress,  $\sigma$ , would be 325 MPa, following from Equation (30), for crankshaft material made of a high-strength iron-based alloy of the following properties summarized in Table 4.

**Table 4.** Summary of the characteristic properties of high-strength iron-based alloy.

Material Property	Value	Reference
Average Modulus of Elasticity	$221 \times 10^9$ Pa	[20]
Average Yield Strength	$359 \times 10^6$ Pa	[20]
Cyclic Hardening Exponent ( $n'$ )	0.135	[20]
Cyclic Hardening Coefficient ( $K'$ )	$1159 \times 10^6$ Pa	[20]

The experimental measurement of the true stress,  $\sigma$ , for the corresponding true strain,  $\epsilon$ , of  $9 \times 10^{-4}$ , is 359 MPa [20]. The comparison of the data of this case study, which is based on fatigue analysis, with the results of the developed model of  $|D_c|$  is statistically analyzed in Table 5 based on Equations (29) and (30).

**Table 5.** Summary of the fatigue analysis.

Table #	$\bar{x}$	$\bar{y}$	$\epsilon_R$
Table 4	326 MPa	359 MPa	9%

The highly dynamic loadings imposed onto the crankshaft indicate how important it is to have an efficient approach of fatigue failure analysis in place; such an approach is presented in the next section.

### 9. Proposed Approach of Fatigue Failure Analysis for Vehicular Dynamic Components

Any fatigue failure occurs through two phases: crack initiation and crack propagation. Thus, for highly dynamic vehicular components, it is suggested to conduct fatigue analysis based on a two-step approach:

i. For the crack initiation phase, a modified version of the local strain approach can be applied. In this proposed approach, notch sensitivity is a key pillar for determining the number of cycles to failure,  $N_f$ . Thus, the proposed approach is as follows:

(i.1.) Determining the notch sensitivity index of the specimen,  $q_f$ , as follows [50]:

$$q_f = \frac{1}{\left(1 + \sqrt{\frac{\alpha}{r}}\right)} \quad (32)$$

where  $\sqrt{\alpha}$  is the Neuber constant, which is a material constant;

$r$  is the radius of curvature of the notch.

(i.2.) Determining the effective stress concentration factor,  $K_f$ , as follows [50]:

$$K_f = \left[ q_f (K_t - 1) \right] + 1 \quad (33)$$

where  $K_t$  is a constant that depends on the type of load and geometry of specimen.

(i.3.) For brittle materials, the fatigue strength,  $\sigma_f$ , with nonzero mean load, alternating applied load and stress concentration, can be determined as follows [50]:

$$\sigma_f = \frac{\sigma_a}{\left[ \frac{1}{K_f} - \frac{\sigma_m}{\sigma_u} \right]} \quad (34)$$

where  $\sigma_a$  is the alternating stress amplitude due to the applied load;

$\sigma_m$  is the mean stress amplitude due to the mean value of the actual load;

$\sigma_u$  is the tensile strength of the material of specimen.

Then, using the determined value of the fatigue strength,  $\sigma_f$ , the corresponding number of cycles to failure,  $N_f$ , is determined from the  $S-N$  curve for the material of the specimen.

(i.4.) For ductile materials, the fatigue strength,  $\sigma_f$ , with nonzero mean load, alternating applied load and stress concentration can be determined as follows [50]:

$$\sigma_f = \frac{K_f \sigma_a}{\left[ 1 - \frac{\sigma_m}{\sigma_u} \right]} \quad (35)$$

Then, using the determined value of the fatigue strength,  $\sigma_f$ , the corresponding number of cycles to failure,  $N_f$ , is also determined from the  $S-N$  curve for the material of the specimen.

ii. For the crack growth phase, a modified version of the fracture mechanics-based approach can be applied. In this proposed approach, within the elastic region of loading, the work performed by the applied loading, " $W_e$ ", is stored as strain energy, " $U$ ", and released upon unloading. However, during fracture, a crack needs energy to propagate, i.e., the work of fracture " $W_f$ ". For a crack size, " $a$ ", a fracture over an infinitesimal distance, " $da$ ", would need an infinitesimal work of fracture, " $dW_f$ ". For the infinitesimal crack, " $da$ ", a fracture will propagate the " $da$ " if disequilibrium takes place and the work performed by the applied loading, " $W_e$ ", is released to permit " $dW_f$ " to occur at a rate that exceeds the critical value such that:

$$\frac{d(W_e - U)}{da} > \frac{dW_f}{da} \quad (36)$$

Thus, the proposed approach in the crack growth phase is as follows:

(ii.1.) Determining the range of the stress intensity factor during a cycle,  $\Delta K$ , which depends on the mode of stress intensity, which in turn depends on the geometry of specimen and the type of loading:

For mode I of stress intensity, in which the specimen has finite width,  $b$ , and the center crack of length " $2a$ " is subjected to tension-based loading [50]:

$$\Delta K = (\sigma_{max} - \sigma_{min}) \left( \sqrt{\pi a} \right) \left( 1 - 0.1 \left( \frac{a}{b} \right)^2 + 0.96 \left( \frac{a}{b} \right)^4 \right) \left( \sqrt{\sec \left( \frac{\pi a}{b} \right)} \right) \quad (37)$$

For mode II of stress intensity, in which the specimen has finite width,  $b$ , and the center crack of length " $2a$ " is subjected to shear-based loading [50]:

$$\Delta K = (\tau_{max} - \tau_{min}) \left( \sqrt{\pi a} \right) \left( 1 - 0.1 \left( \frac{a}{b} \right)^2 + 0.96 \left( \frac{a}{b} \right)^4 \right) \left( \sqrt{\sec \left( \frac{\pi a}{b} \right)} \right) \quad (38)$$

For mode III of stress intensity, in which the specimen has finite width,  $b$ , and the center crack of length " $2a$ " is subjected to out-of-plane shear-based loading [50]:

$$\Delta K = (\tau_{max} - \tau_{min}) \left( \sqrt{\pi a} \right) \left( \sqrt{\left( \frac{b}{\pi a} \right) \tan \left( \frac{\pi a}{b} \right)} \right) \quad (39)$$

(ii.2.) Determining the fatigue crack growth rate ( $da/dN$ ), which is the number of load cycles necessary for a material flaw of subcritical size to grow to the critical size [50]:

$$\frac{da}{dN} = A(\Delta K)^n \quad (40)$$

where  $a$  is the flaw size,  $N$  is the number of load cycles, and  $A$  and  $n$  are material constants.

The stress intensity factor at the critical size,  $K_c$ , is also a material constant at which the flaw size, " $a$ ", becomes the critical size of the flaw, " $a_c$ ". For improving the performance of the crankshaft and to prolong its service life under such dynamic loadings, an innovative nanostructure of the crankshaft is proposed.

## 10. Proposed Nanostructure of Crankshaft for Improved Structural Mechanics

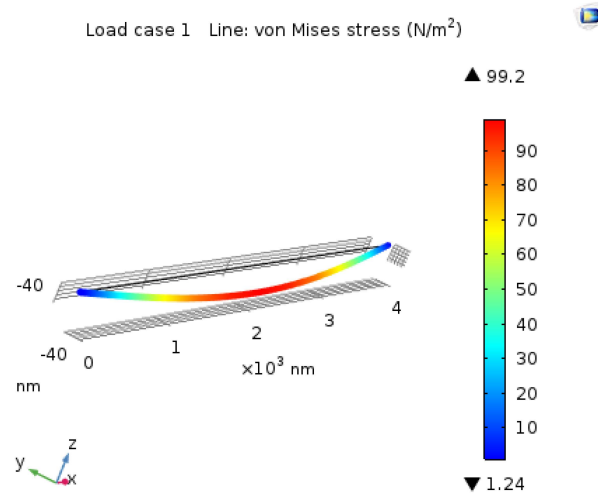
The sensitivity analysis conducted in Section 6 indicated that the dynamic displacement in the flexible crankshaft,  $|D_c|$ , is sensitive to the changes in its independent variables. This sensitivity can be significantly remedied by utilizing an efficient structural material for the crankshaft. Actually, all types of the macroscopic load eventually translate into two types of stress at the nanoscale: normal stress and shear stress. Recently, nanotubes were proposed as a structural strengthening element in the alloy structure of some vehicular structures. However, for withstanding each type of nanoscale stress, more recently the nano-I-beam structure has been innovated outperforming efficiently the nanotube due to the exceptional geometry of the nano-I-beam [51]. Thus, the nano-I-beam is proposed to be added into the alloy structure of the crankshaft. Furthermore, nano-I-beams is proposed

to be used as nanofibers in nanocomposite-based crankshafts. Such a nano-I-beam-based structure can help in reducing induced stresses and hence prolonging the service life of the crankshaft [51].

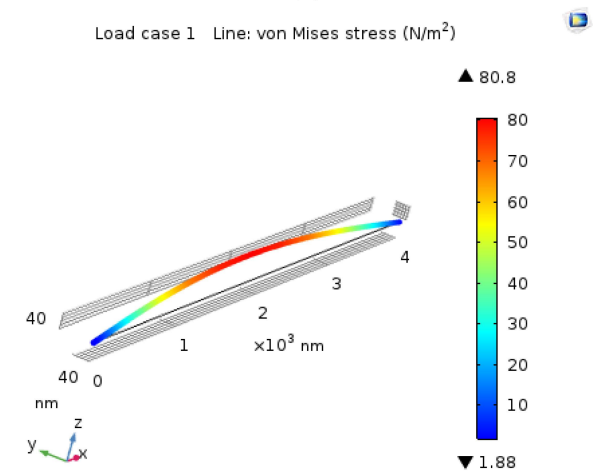
Graphene is proposed to be the structural material of the nano-I-beam in this regard. Graphene is an atomic-scale, 2D hexagonal lattice made of carbon atoms [52]. In addition to the merit of the vibrational damping effect of carbon, graphene meritoriously exhibits exceptional elastic properties and thermodynamic properties due to its C-C hybridized covalent bonds. Thus, the mechanical properties of carbon-based materials, such as the strength of the in-plane  $sp^2$  hybridized  $\sigma$ -bonds in graphene, are much better than those found in several inorganic materials. In this  $sp^2$  hybridization, all the unstable carbon atoms become bonded via  $sp^2$  hybridization so that they get closer to possessing the kinetically favorable state of having all valence orbitals filled as noble gases based on the octet rule [53]. Therefore, it is proposed to have the option of bi-layer nano-fabrics of Graphene-based nano-I-beams with  $90^\circ$  twist stacking angle between the layers in metallic matrix nanocomposite-based crankshafts for enabling structural self-healing and long service life. Moreover, it is proposed to have the option of hybridization of the use of nano-I-beams as nanofibers and nano-fabrics of bi-layer Graphene with  $90^\circ$  twist stacking angle between the layers in metallic matrix nanocomposite-based crankshafts for enabling structural self-healing and long service life.

In this section, the nano-I-beam is thus compared to the nanotube with respect to strength and corresponding induced stresses using finite element analysis based on the core computational engine of COMSOL Multiphysics. Using the finite element analysis, Papanikos et al. [54] evaluated the geometrical characteristics and elastic properties of hollow cylinders as equivalent to carbon nanotubes, concluding that the hollow cylinder shows an equivalent beam to the carbon nanotube. Thus, considering the design of beams for structural strength, the Bernoulli–Euler theory is a key reference in this regard. Therefore, two cross-sections are compared herein: circular tube and I-like shaped beam. For ensuring an accurate and fair comparison, the same value of cross-sectional area is consistently used.

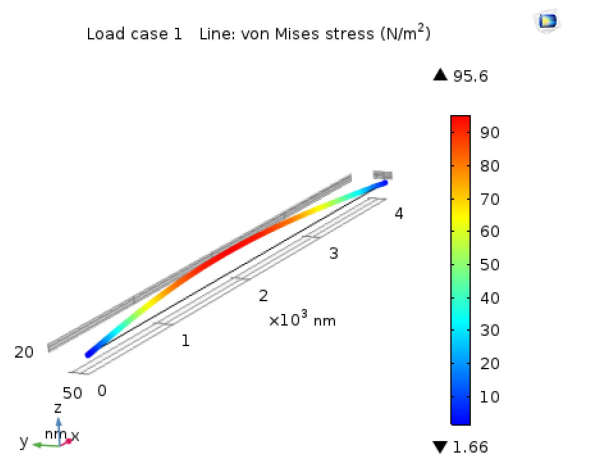
In the finite element models, the standard aspect ratios of the standard sections have been used: (i) for the wide flange I-beam (i.e., w-beam), the European Standard Beams HE 120 A; and (ii) for the equal/near-equal flange and web I-beam (i.e., H-beam), the American Standard Beams AISC W5  $\times$  16. A nanotube is often 15 nanometers wide (i.e.,  $b = 15$  nm) [55]. Thus, the outer radius of the circular tube is  $r_o = 7.5$  nm. By applying the equally corresponding cross-sectional area on the nanotube, the inner radius of the nanotube is  $r_i = 6.3$  nm. The length of the nanotube is typically 4 micrometers = 4000 nm [55], which is the same length as the nano-I-beam. The graphite sheet used in the finite element modeling is characterized in terms of the following properties [56]: Young's modulus = 15.8 GPa; Poisson's ratio = 0.2. The results of this finite element analysis are shown in Figure 3.



(A)



(B)



(C)

**Figure 3.** The Finite Element Analysis for the Two Cross-Sections on Structural Strength. (A) Maximum Induced Stress of Graphite Sheet Nanotube Section; (B) Maximum Induced Stress of Graphite Sheet Wide Flange Nano-I-beam Section; (C) Maximum Induced Stress of Graphite Sheet Equal Flange & Web Nano-I-beam Section.

## 11. Discussion

The present paper has presented analytical modeling of diesel engines, taking the flexibility of the crankshaft into account. The effect of eccentricity in the flexible crankshaft on crankshaft and piston secondary motion has been investigated. The  $e_c$  has been hence analytically modeled in Equation (10) as the summation of the  $e_{HD}$  and  $e_{DM}$ . The  $|D_c|$  has been thus analytically modeled in Equation (25). The sensitivity analysis of the analytical model of the dynamic displacement,  $|D_c|$ , which is summarized in Table 1, shows that the  $|D_c|$  is sensitive to the changes in the independent variables of Equation (25). Following from the sensitivity analysis presented in Table 1, the most influential parameters on the dynamic displacement of the center of the flexible crankshaft due to vibration are the natural frequency and the eccentricity of the crankshaft.

The experimental validation of the analytical model of the  $|D_c|$ , which is indicated in Table 3 based on the eccentricity of crankshaft ( $e_c$ ), shows  $\varepsilon_R$  of 4%, which is less than that of widely recognized models in the field of vehicle powertrains modeling, such as the CMEM and GT-Power. In addition, this relative error of 4% is less than more recently developed models such as Yin's model of the diesel engine, which produces an error of 18% [57]. This relative error of 4% is less than the relative error produced by the CMEM modeler, which indicates a deviation of more than 10% from field data [16,58]. Moreover, this relative error of 4% is less than the relative error produced by the GT-Power modeler, which indicates a deviation of about 5% from field data [59]. Also, the analytical modeling of the  $|D_c|$  has been validated using another experimental case study based on fatigue analysis of the crankshaft, showing a relative error of 9%, as demonstrated in Table 5. The value of the relative error of 9%, in comparison with the 4% error, can be explained in light of the fact that the Ramberg–Osgood relationship itself, i.e., Equation (30), produces such discrepancies in comparison with experimental measurements, particularly at the low values of true strain of  $9 \times 10^{-4}$  and less, which is the case here [49]. This relative error of 9% remains less than the relative error of other relevant models, such as Newman's model of diesel engine fuel consumption, which produces a relative error of 20% [60]. Furthermore, the produced relative errors of 4% and 9% remain in average less than the relative error of other relevant models, such as Lansky's model of the cylinder of diesel engines, which produces a relative error of 15% [61]. Such models developed in the present study would help in reducing diesel engine fuel consumption and exhaust emissions in support of the UN's sustainable development goal of sustainable mobility [62].

The highly dynamic loadings imposed onto the crankshaft indicate how important it is to have in place an efficient approach of fatigue failure analysis for such a vehicular dynamic component. Hence, the proposed approach of fatigue failure analysis for vehicular dynamic components in Section 9 would help in efficiently dealing with such highly dynamic loadings. In addition, the proposed structural nanomaterial of nano-I-beam for the crankshaft has shown meritorious characteristics. Figure 3 indicates that the nano-I-beam provides smaller induced stresses and, thus, a longer service life than nanotubes. Thus, it is recommended to add the structural strengthening elements of graphene nano-I-beams into the alloying structural elements of crankshafts and also into the matrix of nanocomposites-based crankshafts. This is particularly practical in light of the fact that, currently, several vehicular structures are made based on the alloying-based structure with nanometer-sized elements. In fact, several studies, such as [63,64], reported the feasibility and merit of nanometer-sized alloying.

## 12. Conclusions

The present paper has reported the following findings:

1. Providing a brief review on the tribological aspects and mechanics of materials of diesel engines, as can be gathered from Section 2;
2. Analyzing the effect of eccentricity in the flexible crankshaft on crankshaft and piston secondary motion, as presented in Section 4;

3. Analytically modeling the eccentricity of the crankshaft as the summation of the hydrodynamic eccentricity and the dynamic mass eccentricity of the crankshaft, as indicated in Equation (10);
4. Analytically modeling the absolute value of the vibrational dynamic displacement of the center of the crankshaft, as can be gathered from Equation (25);
5. Analyzing based on a sensitivity analysis how sensitive the analytical model of the dynamic displacement in the flexible crankshaft, developed in Equation (25), is to the changes in its independent variables, as presented in Section 6;
6. Analytical modeling of the dynamic displacement in the flexible crankshaft, developed in Equation (25), was validated using an experimental case study based on the eccentricity of the crankshaft showing a relative error of 4%, as can be gathered from Section 7;
7. Analytical modeling of the dynamic displacement in the flexible crankshaft, developed in Equation (25), was validated using another experimental case study based on fatigue analysis showing a relative error of 9%, as indicated in Section 8;
8. A proposed approach of fatigue failure analysis for vehicular dynamic components, as presented in Section 9;
9. A proposed nanostructure of crankshafts for improved structural mechanics, as can be gathered from Section 10.

The reported relative error in the developed models in the present paper is less than the corresponding relative error in several other widely known models. The  $|D_c|$  has been hence analytically modeled and experimentally validated based on the  $e_c$  using a case study with a relative error,  $\varepsilon_R$ , of 4%, which is less than that of key models such as the CMEM and GT-Power. Furthermore, the analytical modeling of the  $|D_c|$  has been validated using another experimental case study based on the fatigue analysis of the crankshaft showing a relative error of 9%, which is less than that of other relevant models, such as Newman's model of diesel engine fuel consumption and Lansky's model of the diesel engine cylinders. The findings of the present research paper indicate that the influence of the flexibility of the crankshaft on the dynamics in the diesel engine is nontrivial. This proposed analytical modeling, analytical approach, and nano-structural material could help in efficiently developing diesel engines, analyzing their performance, and prolonging their service life.

**Author Contributions:** Conceptualization, S.A.M.E.; methodology, S.A.M.E.; analysis, S.A.M.E.; resources, S.A.M.E.; writing—original draft preparation, S.A.M.E.; supervision and review, W.F.F. and H.A.R.; project administration and funding acquisition, W.F.F. and H.A.R. All authors have read and agreed to the published version of the manuscript.

**Funding:** This research received funding from the Center for Sustainable Mobility, Virginia Polytechnic Institute and State University, USA. Also, this research received funding from the IIUM, Malaysia, grant # RMGS 09-10.

**Data Availability Statement:** The data presented in this study are available on request from the corresponding author.

**Acknowledgments:** The International Islamic University Malaysia (IIUM) and Virginia Polytechnic Institute and State University (Virginia Tech) are thanked for their support. In addition, the support provided by the University of Coimbra and the Foundation for Science and Technology (FCT) is acknowledged.

**Conflicts of Interest:** The authors declare no conflict of interest.

## References

1. Preetham, B.S.; Anderson, M.; Richards, C. Mathematical modeling of a four-stroke resonant engine for micro and mesoscale applications. *J. Appl. Phys.* **2014**, *116*, 214904. [[CrossRef](#)]
2. Prakash, R.; Singh, R.K.; Murugan, S. Experimental studies on combustion, performance and emission characteristics of diesel engine using different biodiesel bio oil emulsions. *J. Energy Inst.* **2015**, *88*, 64–75. [[CrossRef](#)]

3. Faris, W.F.; Rakha, H.A.; Elmoselhy, S.A.M. Analytical model of diesel engines exhaust NOx emission rate. *Int. J. Veh. Syst. Model. Test.* **2014**, *9*, 264–280. [CrossRef]
4. Faris, W.F.; Rakha, H.A.; Elmoselhy, S.A.M. Impact of intelligent transportation systems on vehicle fuel consumption and emission modelling: An overview. *SAE Trans. Int. J. Mater. Manuf.* **2014**, *7*, 129–146. SAE Paper # 2013-01-9094. [CrossRef]
5. Faris, W.F.; Rakha, H.A.; Elmoselhy, S.A.M. Validated analytical modeling of diesel engine regulated exhaust CO emission rate. *Adv. Mech. Eng.* **2016**, *8*, 1–15. [CrossRef]
6. Elmoselhy, S.A.M.; Faris, W.F.; Rakha, H.A. Validated analytical modeling of diesel engines intake manifold with a flexible crankshaft. *Energies* **2021**, *14*, 1287. [CrossRef]
7. Elmoselhy, S.A.M.; Faris, W.F.; Rakha, H.A. Experimentally validated analytical modeling of diesel engine power and in-cylinder gas speed dynamics. *J. Mech. Sci. Technol.* **2016**, *30*, 4725–4734. [CrossRef]
8. Kumar, M.; Prajapati, S. Crankshaft design optimality and failure analysis: A review. *Int. J. Sci. Res.* **2017**, *6*. [CrossRef]
9. Hongwei, Y.; Jin, Y.; Baocheng, Z. Analysis of the influences of piston crankshaft offset on piston secondary movements. *Open Mech. Eng. J.* **2015**, *9*, 933–937. [CrossRef]
10. Milasinovic, A.; Filipovic, I.; Hribernik, A. Contribution to the definition of the torsional stiffness of the crankshaft of a diesel engine used in heavy-duty vehicles. *Proc. IMechE Part D J. Automob. Eng.* **2009**, *223*, 921–930. [CrossRef]
11. Fonte, M.; Infante, V.; Reis, L.; Freitas, M. Failure mode analysis of a diesel motor crankshaft. *Eng. Fail. Anal.* **2017**, *82*, 681–686. [CrossRef]
12. Kim, W.; Lee, S. Investigation of torsional vibration characteristics of marine diesel engine crankshaft system. In Proceedings of the 14th International Congress on Sound & Vibration (ICSV14), Cairns, Australia, 9–12 July 2007.
13. Giakoumis, E.G.; Rakopoulos, C.D.; Dimaratos, A.M. Study of crankshaft torsional deformation under steady-state and transient operation of turbocharged diesel engines. *Proc. IMechE Part K J. Multi-Body Dyn.* **2008**, *222*, 17–30. [CrossRef]
14. Elmoselhy, S.A.M.; Faris, W.F.; Rakha, H.A. Validated analytical modelling of supercharging centrifugal compressors with vaneless diffusers for H<sub>2</sub>-biodiesel dual-fuel engines with cooled EGR. *Int. J. Hydrogen Energy* **2017**, *42*, 26771–26786. [CrossRef]
15. Wróblewski, P.; Iskra, A. Problems of reducing friction losses of a piston-ring-cylinder configuration in a combustion piston engine with an increased isochoric pressure gain. In Proceedings of the SAE Powertrains, Fuels & Lubricants Meeting, Krakow, Poland, 22–24 September 2020. SAE Technical Paper # 2020-01-2227. [CrossRef]
16. Rakha, H.A.; Ahn, K.; Faris, W.; Moran, K.S. Simple vehicle powertrain model for modeling intelligent vehicle applications. *IEEE Trans. Intell. Transp. Syst.* **2012**, *13*, 770–780. [CrossRef]
17. Faris, W.F.; Rakha, H.A.; Elmoselhy, S.A.M. Supercharged diesel powertrain intake manifold analytical model. *Int. J. Veh. Syst. Model. Test.* **2014**, *9*, 1–35. [CrossRef]
18. Song, W.; Liu, X.; Berto, F.; Razavi, S. Low-cycle fatigue behavior of 10CrNi3MoV high strength steel and its undermatched welds. *Materials* **2018**, *11*, 661. [CrossRef]
19. Garrison, W.; Banerjee, M. Martensitic Non-Stainless Steels: High Strength and High Alloy, Reference Module in Materials Science and Materials Engineering. In *Encyclopedia of Materials: Science and Technology*; Elsevier: Amsterdam, The Netherlands, 2018. [CrossRef]
20. Williams, J.; Fatemi, A. *Fatigue Performance of Forged Steel and Ductile Cast Iron Crankshafts*; SAE Technical Paper No. 2007-01-1001; Society of Automotive Engineers: Warrendale, PA, USA, 2007.
21. Patil, A.; Datar, G.; Kolhe, A. Crankshaft failure due to fatigue—A review. *Int. J. Mech. Eng. Rob. Res.* **2014**, *3*, 166–172.
22. Bhosale, S.; Chunekar, P.; Gharat, P.; Sirsikar, S. A review of optimization and analysis of crankshaft for passenger car. *J. Emerg. Technol. Innov. Res.* **2019**, *6*, 101–105.
23. DNV GL corporation, Calculation of Crankshafts for Reciprocating Internal Combustion Engines, DNVGL-CG-0037. November 2015. Available online: <https://rules.dnv.com/docs/pdf/DNV/CG/2015-11/DNVGL-CG-0037.pdf> (accessed on 27 April 2022).
24. Aliakbaria, K.; Imanparastb, M.; Nejad, R. Microstructure and fatigue fracture mechanism for a heavy-duty truck diesel engine crankshaft. *Sci. Iran. B* **2019**, *26*, 3313–3324. [CrossRef]
25. Witek, L.; Stachowicz, F.; Załęski, A. Failure investigation of the crankshaft of diesel engine. *Procedia Struct. Integr.* **2017**, *5*, 369–3768. [CrossRef]
26. Kubo, H.; Mori, H. Technical Developments and Recent Trends in Crankshaft Materials. *Kobelco Technol. Rev.* **2005**, *26*, 37–42. Available online: [https://www.kobelco.co.jp/english/ktr/pdf/ktr\\_26/037-042.pdf](https://www.kobelco.co.jp/english/ktr/pdf/ktr_26/037-042.pdf) (accessed on 27 April 2022).
27. Pawar, P.; Dalvi, S.; Rane, S.; Divakaran, C.B. Evaluation of crankshaft manufacturing methods—An overview of material removal and additive processes. *Int. Res. J. Eng. Technol.* **2015**, *2*, 118–122. Available online: <https://www.irjet.net/archives/V2/i4/Irjet-v2i421.pdf> (accessed on 27 April 2022).
28. Khonsari, M. Chapter 61. Journal bearing design and analysis. In *Tribology Data Handbook*; CRC Press: Boca Raton, FL, USA, 1997.
29. The Society of Tribologists and Lubrication Engineers (STLE) Alberta Section. *Basic Handbook of Lubrication*, 2nd ed.; The Society of Tribologists and Lubrication Engineers: Park Ridge, IL, USA, 2003.
30. Sander, D.E.; Allmaier, H.; Priebsch, H.H.; Witt, M.; Skiadas, A. Simulation of journal bearing friction in severe mixed lubrication—Validation and effect of surface smoothing due to running-in. *Tribol. Int.* **2016**, *96*, 173–183. [CrossRef]
31. Uzoma, P.C.; Hu, H.; Khadem, M.; Penkov, O.V. Tribology of 2D nanomaterials: A review. *Coatings* **2020**, *10*, 897. [CrossRef]
32. Xu, M.; Liang, T.; Shi, M.; Chen, H. Graphene-like two-dimensional materials. *Chem. Rev.* **2013**, *113*, 3766–3798. [CrossRef] [PubMed]

33. Cho, Y.; Park, J.; Ku, B.; Lee, J.; Park, W.; Lee, J.; Kim, S.H. Synergistic effect of a coating and nano-oil lubricant on the tribological properties of friction surfaces. *Int. J. Precis. Eng. Manuf.* **2012**, *13*, 97–102. [CrossRef]
34. Arif, M.; Shukla, D.K.; Kango, S.; Sharma, N. Implication of surface texture and slip on hydrodynamic fluid film bearings: A comprehensive survey. *Tribol. Online* **2020**, *15*, 265–282. [CrossRef]
35. Schüler, E.; Berner, O. Improvement of tilting-pad journal bearing operating characteristics by application of eddy grooves. *Lubricants* **2021**, *9*, 18. [CrossRef]
36. Gropper, D.; Wang, L.; Harvey, T. Hydrodynamic lubrication of textured surfaces: A review of modeling techniques and key findings. *Tribol. Int.* **2016**, *94*, 509–529. [CrossRef]
37. Chernets, M.; Pashechko, M.; Kornienko, A.; Buketov, A. Study of the influence of temperature on contact pressures and resource of metal-polymer plain bearings with filled Polyamide PA6 bushing. *Lubricants* **2022**, *10*, 13. [CrossRef]
38. Childs, P.R.N. *Chapter 2: Mechanical Design*, 3rd ed.; Butterworth-Heinemann: Oxford, UK; Elsevier Ltd.: Amsterdam, The Netherlands, 2021. [CrossRef]
39. Suh, N.P. *Tribophysics*; Prentice-Hall: Englewood Cliffs, NJ, USA, 1986.
40. Neale, M.J. *The Tribology Handbook*, 2nd ed.; Butterworth-Heinemann: Oxford, UK, 2001.
41. Stolarski, T.A. *Tribology in Machine Design*; Butterworth-Heinemann: Oxford, UK, 2000.
42. Chowdhury, M.A.; Mia, M.S.; Kchaou, M.; Shuvho, M.B.A.; Debanath, U.K. Friction coefficient and performance evaluation of plain journal bearing using SAE 5W-30 engine oil. *Proc IMechE Part J J. Eng. Tribol.* **2020**, *234*, 1222–1232. [CrossRef]
43. Sadabadi, H.; Nezhad, A.S. Nanofluids for performance improvement of heavy machinery journal bearings: A simulation study. *Nanomaterials* **2020**, *10*, 2120. [CrossRef] [PubMed]
44. Vinogradov, O. *Fundamentals of Kinematics and Dynamics of Machines and Mechanisms*; CRC Press: Boca Raton, FL, USA, 2000.
45. U.S. Environmental Protection Agency EPA. *Process for Conducting Probabilistic Risk Assessment*; Appendix A, Rags; Environmental Protection Agency EPA: Washington, DC, USA, 2001; Volume 3, Part A.
46. Fedák, V.; Záskalický, P.; Gelvanič, Z. Analysis of Balancing of Unbalanced Rotors and Long Shafts using GUI MATLAB. Chapter 19 in the Edited Book. *MATLAB Applications for the Practical Engineer*. InTech Open. 2014, pp. 535–564. Available online: <https://api.intechopen.com/chapter/pdf-download/46862> (accessed on 27 April 2022). [CrossRef]
47. Zemin, F.; Guangming, L. Simulative analysis for static and dynamic behavior of QT800-2ductile iron crankshaft. *Optoelectron. Adv. Mater. Rapid Commun.* **2014**, *8*, 115–120. Available online: <http://oam-rc2.inoe.ro/articles/simulative-analysis-for-static-and-dynamic-behaviour-of-qt8002-ductile-iron-crankshaft/fulltext> (accessed on 27 April 2022).
48. Keller, G. *Statistics for Management and Economics, South Western*, 9th ed.; Cengage Learning: Boston, MA, USA, 2012.
49. Patwardhana, P.; Nalavdea, R.; Kujawski, D. An estimation of Ramberg-Osgood constants for materials with and without Luder's strain using yield and ultimate strengths. *Procedia Struct. Integr.* **2019**, *17*, 750–757. [CrossRef]
50. Pilkey, W.D. *Chapter 6. Formulas for Stress, Strain, and Structural Matrices*, 2nd ed.; John Wiley & Sons, Inc.: Hoboken, NJ, USA, 2008.
51. Elmoselhy, S.A.M. Hybrid organic/inorganic nano-I-beams for structural nano-mechanics. *Nat. Sci. Rep.* **2019**, *9*, 18324. [CrossRef] [PubMed]
52. Kis, A.; Mihailovic, D.; Remskar, M.; Mrzel, A.; Jesih, A.; Piwonski, I.; Kulik, A.J.; Benoit, W.; Forro, L. Shear and Young's moduli of MoS<sub>2</sub> nanotube ropes. *Adv. Mater.* **2003**, *15*, 733–736. [CrossRef]
53. Višić, B.; Panchakarla, L.S.; Tenne, R. Inorganic nanotubes and fullerene-like nanoparticles at the crossroads between solid-state chemistry and nanotechnology. *J. Am. Chem. Soc.* **2017**, *139*, 12865–12878. [CrossRef] [PubMed]
54. Papanikos, P.; Nikolopoulos, D.D.; Tserpes, K.I. Equivalent beams for carbon nanotubes. *Comput. Mater. Sci.* **2008**, *43*, 345–352. [CrossRef]
55. Frank, S.; Poncharal, P.; Wang, Z.L.; de Heer, W.A. Carbon nanotube quantum resistors. *Science* **1998**, *280*, 1744–1746. [CrossRef]
56. AZO Materials, "Carbon-Graphite Materials". Available online: <https://www.azom.com/properties.aspx?ArticleID=516> (accessed on 23 March 2019).
57. Yin, J.; Su, T.; Guan, Z.; Chu, Q.; Meng, C.; Jia, L.; Wang, J.; Zhang, Y. Modeling and validation of a diesel engine with turbocharger for hardware-in-the-loop applications. *Energies* **2017**, *10*, 685. [CrossRef]
58. Rakha, H.; Ahn, K.; Trani, A. Comparison of Mobile5a, VT-Micro, and CMEM models for estimating hot stabilized light duty gasoline vehicle emissions. *Can. J. Civ. Eng.* **2003**, *30*, 1010–1021. [CrossRef]
59. Bos, M. Validation Gt-Power Model Cyclops Heavy Duty Diesel Engine. Master's Thesis, The Technical University of Eindhoven, Eindhoven, The Netherlands, 2007.
60. Newman, P.W.G.; Alimoradian, B.; Lyons, T.J. Estimating fleet fuel consumption for vans and small trucks. *Transp. Sci.* **1989**, *23*, 46–50. [CrossRef]
61. Lansky, L. Diesel Engine Modelling and Control. Master's Thesis, Czech Technical University in Prague, Prague, Czech Republic, 2008.
62. Elmoselhy, S.A.M.; Faris, W.F.; Rakha, H.A. Experimentally validated analytical modeling of diesel exhaust HC emission rate. *J. Mech. Sci. Technol.* **2014**, *28*, 4139–4149. [CrossRef]
63. Zhang, H.; Liu, T.; Zhao, S.; Xu, Z.; Lv, Y.; Fan, J.; Han, Y. Size-Dependent alloying ability of immiscible W-Cu bimetallic nanoparticles: A theoretical and experimental study. *Nanomaterials* **2021**, *11*, 1047. [CrossRef]
64. Lee, J.G.; Mori, H.; Yasuda, H. Alloy phase formation in nanometer-sized particles in the In-Sn system. *Phys. Rev. B* **2002**, *65*, 132106. [CrossRef]